The mechanics of surficial failure in soil slopes

Poul V. Lade *

Department of Civil Engineering, The Catholic University of America, Washington, D.C. 20064, USA

ABSTRACT

It is not safe to employ the classical infinite slope failure analysis procedure in which the Coulomb failure criterion is used, because a very large portion of the factor of safety is assigned to the effective cohesion which is not present in the soil. Part of the problem arises from the normal stresses used in the drained direct shear tests, which are high relative to the normal stresses prevailing in surficial failures. The real effective strength envelope is curved, and it is proposed to model it by a power function whose parameter values may be determined from the usual shear tests performed at the normal stress magnitudes usually employed. Based on the factor of safety calculations from the curved failure envelope and observations from field rainfall infiltration experiments, the mechanics of surficial failure of slopes is explained.

© 2010 Elsevier B.V. All rights reserved.

1. Introduction

The surficial stability of slopes is seriously affected by rainfall, because the shear strength that is present in unsaturated soils due to matric suction is lost as a result of rainwater infiltration into the soil. While surficial failures of soil slopes may happen anywhere, they tend to attract more attention in semi-arid areas of the world in which the upper layer of the soil dries out for some years followed by a year with heavy rainfalls which saturate the upper layers and cause a large number of surficial failures. In Southern California the annual precipitation typically varies from 25 to 50 cm (10 to 20 in.) of water with an average of about 38 cm (15 in.) and most of the rainfalls occur in the winter months. In some years the rainfall increases to unusual magnitudes. Based on data from the National Weather Service, the Los Angeles Times reports annual above-normal winter rains (measured from July 1 to June 30) as follows:

1940–41: 81.2 cm (32.76 in.)
1968–69: 69.8 cm (27.47 in.)
1977–78: 84.9 cm (33.44 in.)
1982–83: 79.4 cm (31.25 in.)
1992–93: 69.5 cm (27.36 in.)
1997–98: 78.7 cm (31.01 in.)

It is during such years of unusual, heavy precipitation that surficial failures occur in large numbers. For example, the third heaviest storm recorded since 1877 occurred in 1977–78 (Los Angeles Times: July 5,

1986), and it produced more than a thousand slope failures in Los Angeles County, a large proportion of which were surficial failures.

In an excellent study of the conditions leading to surficial failure, Pradel and Raad (1993) found that the rainfall has to be sufficiently intense to exceed the infiltration rate of the soil and it has to be sufficiently heavy to saturate the slope. Pradel and Raad (1993) indicated that the permeability of the soil plays a role in the susceptibility to surficial failure. They argued that soils with permeabilities above a certain limiting value would not become saturated, and slopes made of sandy and gravelly soils would therefore not exhibit surficial instability. Rather, it was the slopes made of clayey and silty soils that would be prone to become unstable, as is in agreement with actual observations made by Hollingsworth and Kovacs (1981).

Surficial failure is most often addressed by an infinite slope stability analysis, as reviewed below. However, the effective cohesion plays an inordinate large role in calculation of the factor of safety by the classical infinite slope analysis. It will be shown that effective cohesion does not exist in non-cemented soils, but rather the failure envelope for soils is curved, and this may be correctly accounted for in the infinite slope stability analysis employed for surficial stability. Finally, experiments on water infiltration into a soil slope performed by Ng and Zhan (2007) are used to indicate the mechanics leading to surficial instability of soil slopes.

2. Classical infinite failure analysis

It is well-known that effective stress analyses in soils can be performed in two different ways using:

(1) Total unit weights and water pressures
   or
(2) Buoyant unit weights and seepage forces

---

* Tel.: +1 202 319 6942; fax: +1 202 319 6677.
 E-mail address: Lade@cua.edu.

Both procedures employ effective strength parameters, c' and φ', and both may be used to find the factor of safety for a saturated, homogeneous, infinite slope (Skempton and DeLory 1957), as shown in Fig. 1(a). The two procedures produce the same answer, but the first procedure is generally more straight-forward (Lambe and Whitman, 1969; Abramson et al., 2002; Duncan and Wright, 2005).

The water enters the slope and is directed parallel to the surface by an impervious layer at some depth. The water table is at the sloping ground surface, the flow lines are parallel to the slope, and the equipotential lines are perpendicular to the slope. The water pressure is therefore zero at the ground surface and it increases with depth as indicated in Fig. 1(a). At the vertical depth h the water pressure is:

$$u = \gamma_w \cdot h \cdot \cos^2 \alpha \qquad (1)$$

The total weight of the block with depth $h \cdot \cos\alpha$ and length b is:

$$W = \gamma_{sat} \cdot b \cdot h \cdot \cos\alpha \qquad (2)$$

in which γ_{sat} is the saturated unit weight of the soil. The side forces parallel to the slope at the two ends of the block are opposite and equal in magnitude in an infinite slope, and they cancel out of the equilibrium considerations.

Thus, only the vertical force W and the water pressures u directed perpendicular to the base are considered in the force equilibrium of the block. The vertical force W is resolved into components parallel and perpendicular to the slope as shown in Fig. 1(b), and these components are then employed in determination of the shear stress and the effective normal stress at the base of the block:

$$\tau = \frac{W \cdot \sin\alpha}{b} = \frac{\gamma_{sat} \cdot b \cdot h \cdot \cos\alpha \cdot \sin\alpha}{b} = \gamma_{sat} \cdot h \cdot \cos\alpha \cdot \sin\alpha \qquad (3)$$

$$\sigma' = \frac{W \cdot \cos\alpha}{b} - u = \frac{\gamma_{sat} \cdot b \cdot h \cdot \cos^2\alpha}{b} - \gamma_w \cdot h \cdot \cos^2\alpha = (\gamma_{sat} - \gamma_w) \cdot h \cdot \cos^2\alpha \qquad (4)$$

The shear strength available at the base of the block according to the Coulomb failure criterion is therefore:

$$s = c' + \sigma' \cdot \tan\phi' = c' + (\gamma_{sat} - \gamma_w) \cdot h \cdot \cos^2\alpha \cdot \tan\phi' \qquad (5)$$

The factor of safety is then calculated as:

$$F = \frac{s}{\tau} = \frac{c' + (\gamma_{sat} - \gamma_w) \cdot h \cdot \cos^2\alpha \cdot \tan\phi'}{\gamma_{sat} \cdot h \cdot \cos\alpha \cdot \sin\alpha} \qquad (6)$$

In this expression $(\gamma_{sat} - \gamma_w)$ is equal to the buoyant unit weight γ_b. For a cohesionless soil, $c' = 0$ and the factor of safety becomes independent of depth h:

$$F = \frac{\gamma_b}{\gamma_{sat}} \cdot \frac{\tan\phi'}{\tan\alpha} \qquad (7)$$

Since the buoyant unit weight, γ_b, is approximately one half of the saturated unit weight, γ_{sat}, the factor of safety is approximately:

$$F \cong \frac{1}{2} \cdot \frac{\tan\phi'}{\tan\alpha} \qquad (8)$$

In comparison, the factor of safety for a completely dry, cohesionless slope is:

$$F = \frac{\tan\phi'}{\tan\alpha} \qquad (9)$$

Failure in a dry sand slope will occur for $F = 1$ at which $\alpha = \varphi' =$ angle of repose. Actual observations indicate that failure occurs by raveling of a thin layer of dry sand right at the sloping ground surface. If the slope is saturated and water seeps parallel to the sloping surface, Eq. (8) indicates that the factor of safety is only half of that for a dry slope in cohesionless soil.

Note that for a soil with effective cohesion, Eq. (6) indicates that the factor of safety decreases with increasing depth, while the factor of safety is independent of depth for a slope without cohesion. Thus, no particular unsafe depth or location at which shear failure will occur is indicated by Eq. (8).

3. The nature of effective cohesion in soils

3.1. Components of shear strength

The shear strength of soils consists of contributions from the granular portion and from the clay size portion of the soil. The
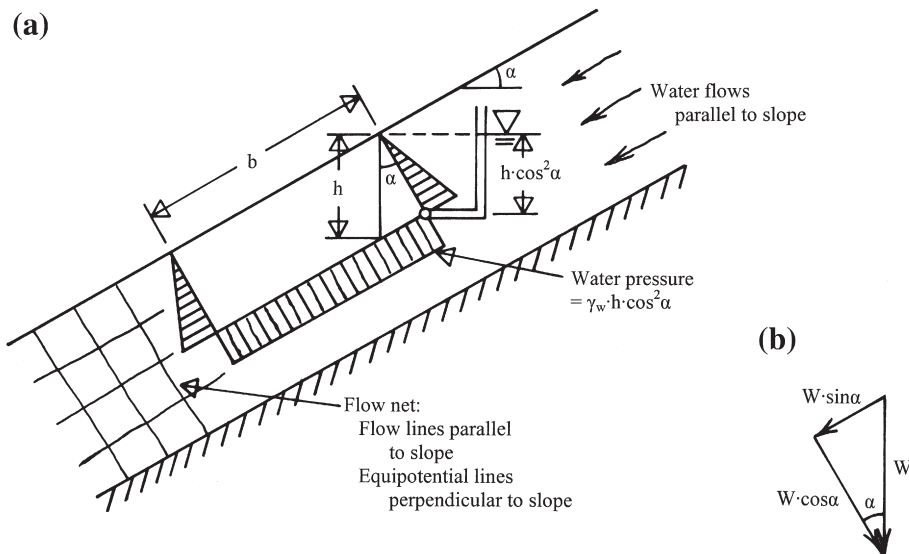
Fig. 1. Surficial stability analysis by total unit weights and water pressures: (a) forces acting on soil block, and (b) resolution of forces parallel and perpendicular to soil slope with inclination α.

granular portion exhibits frictional resistance due to basic friction between particles, interlocking resistance due to energy required to produce volume expansion (dilation), to rearrange particles at constant volume, and to crush particles. The contribution due to interlocking resistance reduces with increasing confining pressure, because rather than moving over each other and causing expansion, the particles begin to crush with increasing pressure. At very high pressures, the frictional resistance between particles prevents the particles from sliding and crushing becomes the primary mode of deformation. As the dilation changes to contraction due to particle crushing at high pressures, the rate of increase in shear strength decreases with increasing normal stresses and the shear strength envelope is therefore curved.

The shearing resistance between clay particles also manifests itself by frictional resistance due to normal stresses between particles. However, since particles of clay minerals are electrically charged, there is a possibility of an additional shearing resistance at zero normal stress due to electrostatic and electromagnetic attractions and possibly due to interparticle bonds as explained by Mitchell and Soga (2005). However, they point out that the magnitude of the resulting effective cohesion, including the adhesion between particles caused by the electrostatic forces, is so small that it cannot be measured in conventional laboratory tests. True cohesion of any significance is therefore not present in soils unless they are cemented.

3.2. Experimental study of effective cohesion

A study of the magnitude of effective cohesion in compacted, clayey soils was performed. A total of 5 clayey soils were selected from a group of 13 soils collected in the greater Los Angeles area for a study of the Expansion Index test (Anderson and Lade, 1981; ASTM Standard Method D 4829, 2006). The index properties of these 5 soils are listed in Table 1, and they are representative of soils that are commonly compacted in slopes in Southern California. Badges of soil passing the #40 U.S. sieve were mixed with water contents 1% higher than the optimum water contents listed in Table 1 and allowed to cure for 48 h before soil specimens were prepared by the modified compaction method (ASTM Standard Method D 1557, 2006). The specimens were compacted in 5 layers using a Harvard miniature compactor to approximately 95% of the maximum dry unit weight in a cylindrical mold with diameter of 35.6 mm (1.4 in.) and height of 102 mm (4.0 in.). After extrusion, the specimens were sealed in air tight containers before testing.

Effective cohesion implies that a soil has shear strength at zero confining pressure. To test for effective cohesion, compacted soil cylinders were placed in 500 ml glass beakers. Water was then added to immerse the specimens to within approximately one centimeter of the top of the specimen. Failure was defined to occur at the instant the specimen fell completely below the water surface in the beaker. A specimen tested as described is essentially under zero effective confining pressure, and the requirements for determination of effective cohesion are therefore fulfilled.

Three specimens were prepared for each of the five soil types. The first set of specimens was air-dried for one week prior to testing. The second set was air-dried for one week and subsequently oven-dried at 110 °C for 24 h. The third set was tested as-compacted at 1% higher than the optimum water content.

With one exception, all air-dried and oven-dried specimens failed within 44 min, as seen from Table 2. The air-dried specimen of soil no. 3 failed within 400 min. Water infiltrated into the specimen thus forming a wetting front that allowed air to escape up through the end open to air above the water surface. Continuous slaking of the specimen surface resulted in reducing diameter until the specimen collapsed. Within another 30 min after failure, the specimens were completely broken down to a fine-grained slurry. These experiments all clearly show that there is no effective cohesion in compacted soils. Thus, effective cohesion cannot be relied upon to help maintain the stability of soil slopes.

The as-compacted specimens were immersed for 20 days. Within this time period soil no. 10 nearly reached failure, while soil no. 6 showed considerable slaking. The other as-compacted specimens showed no sign of distress other than minor expansion and cracking. At water contents of 1% above the optimum water contents and at 95% relative compaction, the degrees of saturation of the specimens were in the range from 71 to 92%, as listed in Table 2. In this range of saturation, the air-phase may not be continuous and the air in the partly saturated soil is present in bubbles in the voids. Surface tension causes the air bubbles to be stable, and they are relatively immovable and tend to block and prevent additional water from intruding into the soil. The water is under tension, and this produces an effective confining pressure, which in turn provides the soil with some frictional strength and results in stability of the soil.

4. Curved failure envelope and its characterization

While it is clear that there is no effective cohesion in soils of any type, the failure envelope is curved, especially at low effective confining pressures. Observed surficial failures occur at depths of 0.5 to 1.5 m (2 to 6 ft). At these depths the effective normal stress is in the order of 5 to 20 kPa (100 to 400 lb/ft^2). This range is well below the range of stresses at which specimens are commonly tested for investigation of slope stability. Strength parameters are usually

Table 1
Index properties of 5 soils tested for effective cohesion.

Soil no.	3	6	9	10	11
Description	Gray brown sandy silt, some clay	Red brown sand, some silt and clay	Brown black silt, sand and clay, well graded	Light brown silt, sand, clay mixture, well graded	Black brown silt, some clay, little sand
Unified classification	MH	ML	ML	ML	MH
Maximum unit weight (modified comp.)	1819 kg/m^3 (113.5 lb/ft^3) at 18.5%	1899 kg/m^3 (118.5 lb/ft^3) at 12%	1867 kg/m^3 (116.5 lb/ft^3) at 12.6%	2043 kg/m^3 (127.5 lb/ft^3) at 10.8%	1611 kg/m^3 (100.5 lb/ft^3) at 20.6%
Liquid limit	57	41	34	30	58
Plastic limit	29	19	15	16	29
Shrinkage limit	21	19	15	18	18
%Clay	18	12	22	30	26
%Passing #200 Sieve	60	40	65	70	83
Activity	2.15	3.14	1.11	0.56	1.38
Expansion index	75	38	56	29	95
Free swell value	85	74	80	70	110
Specific gravity	2.69	2.71	2.69	2.76	2.67
Mineralogy by X-ray diffraction	Quartz, feldspar, montmorillonite, heulandite (a zeolite)	Quartz, feldspar, montmorillonite, unknown mineral	Quartz, feldspar, montmorillonite	Quartz, feldspar, montmorillonite, illite	Quartz, feldspar, montmorillonite, illite

Table 2
Results of immersion tests for all compacted soil specimens.

Soil no.	Relative compaction = % of maximum dry unit weight	Time-to-failure (min)
Air-dried specimens		
3	94.2	<400
6	96.3	26
9	96.0	35
10	95.1	42
11	95.8	16
Oven-dried specimens		
3	94.0	25
6	96.0	21
9	96.3	44
10	95.4	29
11	95.5	35
As-compacted specimens ($w = w_{opt} + 1\%$)		
3	94.2 ($S = 92.0\%$)	No failure
6	95.5 ($S = 71.3\%$)	No failure
9	95.7 ($S = 72.4\%$)	No failure
10	94.9 ($S = 76.9\%$)	Nearly failed
11	95.1 ($S = 77.6\%$)	No failure

obtained with minimum values of effective normal stresses of approximately 50 kPa (1000 lb/ft²). A typical example of results of direct shear tests on compacted soil is shown in Fig. 2. The effective strength envelope for compacted soils and for soils without true cementation goes through the stress origin and is curved as indicated in Fig. 2. Passing a best-fit straight line through the experimental points will indicate an effective cohesion, but this is clearly not correct. The Coulomb failure criterion with strength parameters c' and φ' from conventional tests overestimates the shear strength available at low normal stresses, often by a factor in the order of 2 in the range of stresses that is important for surficial failure analysis. The results of direct shear tests interpreted in terms of the Coulomb failure criterion are not appropriate for evaluating of surficial slope stability, because the range of effective normal stresses in the field is not used in the laboratory tests.

The curved effective strength failure envelope without effective cohesion may be modeled by a power function of the following simple form:

$$\left(\frac{s}{p_a}\right) = a \cdot \left(\frac{\sigma'}{p_a}\right)^b \tag{10}$$

or

$$s = a \cdot p_a \cdot \left(\frac{\sigma'}{p_a}\right)^b \tag{11}$$
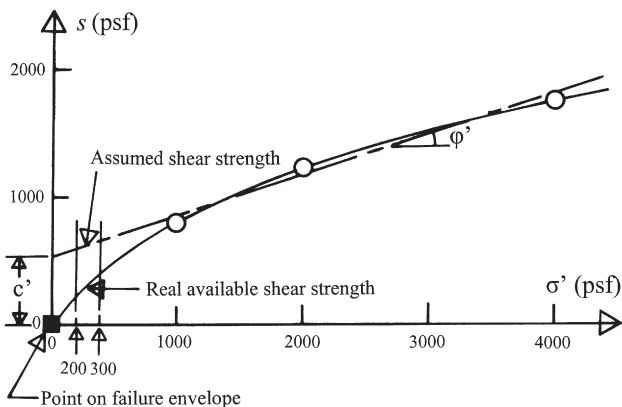
Fig. 2. Modeling of shear strength envelope by the Coulomb failure criterion, while the real failure surface goes through the stress origin (1 psf = 0.049 kPa).

in which a and b are dimensionless numbers and p_a is the atmospheric pressure in the same units as s and σ' ($p_a = 1.0$ atm ≈ 1.0 kg/cm² ≈ 14.2 psi ≈ 2050 psf ≈ 100 kPa). To find the values of a and b, the logarithm is taken on both sides of Eq. (10) to produce an expression that depicts a straight line on a log–log diagram:

$$\log\left(\frac{s}{p_a}\right) = \log a + b \cdot \log\left(\frac{\sigma'}{p_a}\right) \tag{12}$$

Fig. 3 shows a schematic log–log diagram with the results from direct shear tests for which a is the value of (s/p_a) at $(\sigma'/p_a) = 1$, and b is the geometric slope of the straight line, as indicated on the diagram.

Table 3 gives the results of 3 direct shear tests on soil no. 9 compacted at 90% of the Modified Proctor maximum dry unit weight, and Fig. 4 shows the parameter determination on a log–log diagram. Parameter values of $a = 0.57$ and $b = 0.54$ are obtained for characterization of the curved failure envelope. The comparison between experimental results and the curved failure envelope is shown on the diagram in Fig. 5. This diagram also shows the best-fit Coulomb failure parameters. It may be seen that the Coulomb failure envelope for the soil overestimates the shear strength by a factor of approximately 2 in the range of normal stresses where surficial failures may occur.

The expression in Eq. (10) was also used to fit the experimental results obtained by Day and Axten (1989). They presented results of drained direct shear tests, including tests performed at low normal stresses, on 5 soils from Southern California compacted at 90% of the Modified Proctor maximum dry density and optimum water contents (ASTM 1557). The best-fit parameters for these 5 soils are given in Table 4, and the fits of the power function failure criterion with the experimental results are shown in Fig. 6.

The direct shear test can only be interpreted in terms of average stresses acting on the shear plane, while the true normal and shear stress distributions are quite nonuniform. However, the expression for the curved failure envelope is also suitable for characterization from results of triaxial compression tests. Table 5 presents the strength results for 3 drained triaxial compression tests on intact specimens of dense, medium to coarse sand. The sand contained sufficient amounts of fines to avoid disintegration and remain intact during extrusion from the sampling rings and installation in the triaxial apparatus. Since τ and σ are stresses on the failure plane in the triaxial specimen, they correspond to the stresses at which the Mohr circle touches the failure envelope. These stresses are not measured in the triaxial test. However, parameter determination does not appear to be very sensitive to accurately estimated values of τ and σ. To obtain the parameters for characterization by a curved failure envelope, the solid data points shown on the Mohr circles in Fig. 7 are estimated to be located on the curved failure envelope, digitized, and plotted on the log–log diagram in Fig. 8. Since these points are estimated, the accuracy of the parameter determination is evaluated by selecting the additional open points, which are located away from
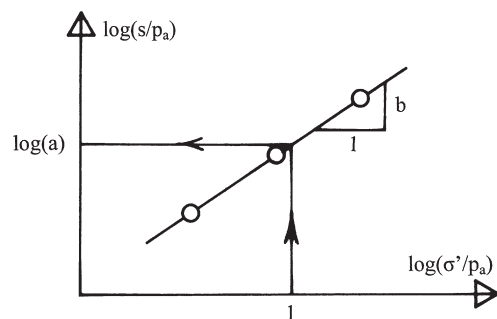
Fig. 3. Schematic diagram of parameter determination for proposed power function failure criterion.

Table 3
Results of 3 direct shear tests on soil no. 9 compacted at 90% of the modified proctor maximum dry unit weight.

Test no.	s (kPa)	σ' (kPa)	s/p_a	σ'/p_a
1	38.2	48.9	0.382	0.488
2	57.1	97.8	0.570	0.977
3	89.2	244.5	0.891	2.442
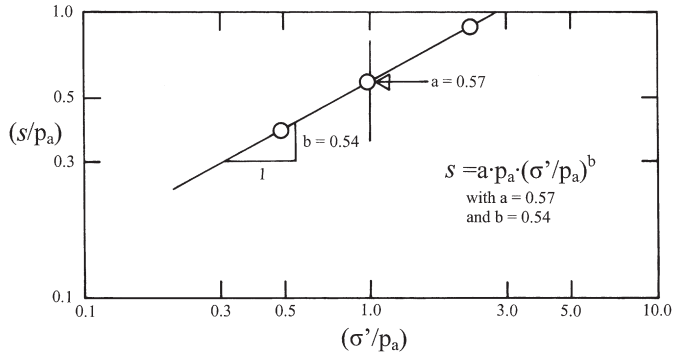
Fig. 4. Parameter determination for power function failure criterion for direct shear tests on soil no. 9.
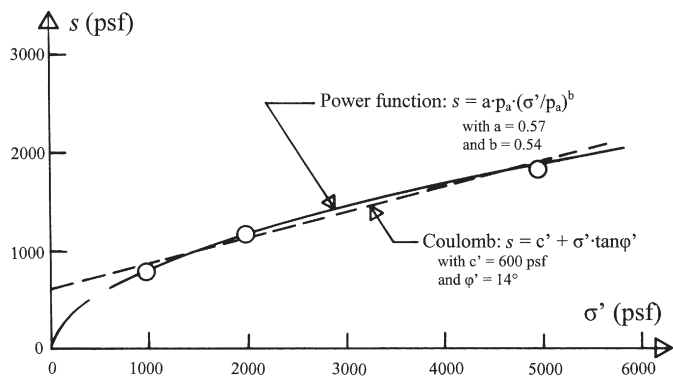
Fig. 5. Comparison of Coulomb failure criterion and power function failure criterion with experimental results for soil no. 9 (1 psf = 0.049 kPa).

the solid points in Fig. 7. These open points are also shown in Fig. 8, and it may be seen that they would not have resulted in substantially different parameter values than those obtained from the solid points. Parameter values of $a = 1.10$ and $b = 0.875$ are obtained for characterization of the curved failure envelope. The comparison between experimental results and the curved failure envelope is shown on the diagram in Fig. 7. This diagram also shows the best-fit Mohr–Coulomb failure parameters. It may be seen that the straight Mohr–Coulomb failure envelope overestimates the shear strength by a factor of at least 2 in the range of normal stresses (10–15 kPa) where surficial failures may occur. Although the triaxial tests were not

Table 4
Non-dimensional parameters a and b for curved failure criterion expressed by power function for 5 compacted soils tested in drained direct shear tests by Day and Axten (1989).

Soil	Parameter a	Parameter b
Capistrano Formation(CL)	0.69	0.76
Point Loma Formation(CL)	0.65	0.76
Topanga Formation(CH)	0.60	0.76
Mission Valley Formation(CL)	0.58	0.71
Friars Formation(CL–CH)	0.56	0.74
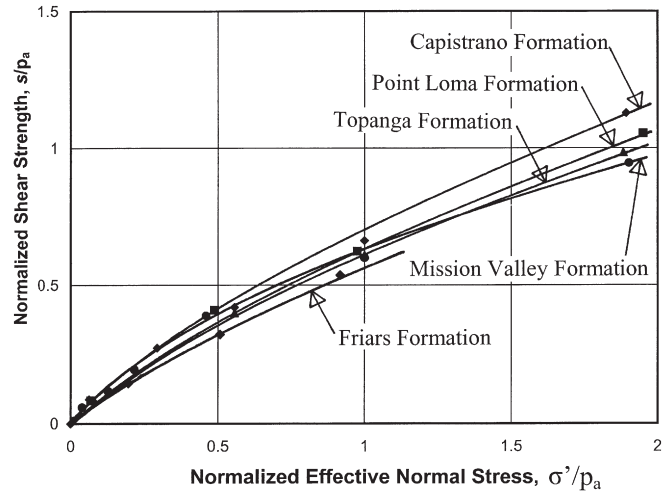
Fig. 6. Comparison of curved failure criterion expressed by power function with experimental results obtained for 5 compacted soils tested in drained direct shear tests by Day and Axten (1989).

Table 5
Results of 3 triaxial compression tests on dense, medium to coarse sand.

Test no.	Depth (m)	σ'_3 (kPa)	$(\sigma_1 - \sigma_3)_{max}$ (kPa)	$\gamma_{d,init}$ (kg/m^3)
1	23.2	50	279	1690
2	24.7	150	720	1755
3	29.3	450	1637	1810

performed in the appropriate range of stress for a surficial failure analysis, the inclusion of the stress origin as a point on the failure envelope helps produce a plausible strength characterization in the entire range of stresses.

The power function in Eq. (10) provides a good model for the curved failure envelopes of many non-cemented soils. It implies zero effective cohesion and a decreasing effective stress friction angle with increasing normal stress. The parameters a and b in the proposed curved failure criterion may be determined from drained direct shear tests or from triaxial compression tests performed at conventional normal stresses.
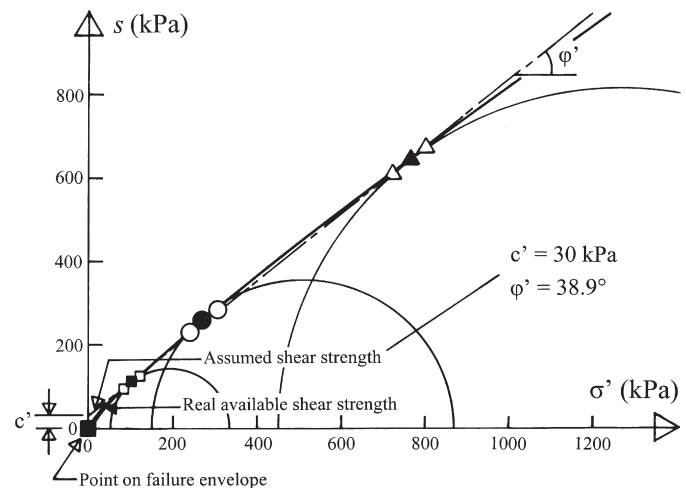
Fig. 7. Mohr circles from triaxial compression tests on dense, medium to coarse sand, and comparison of Mohr–Coulomb failure criterion and power function criterion with experimental results.
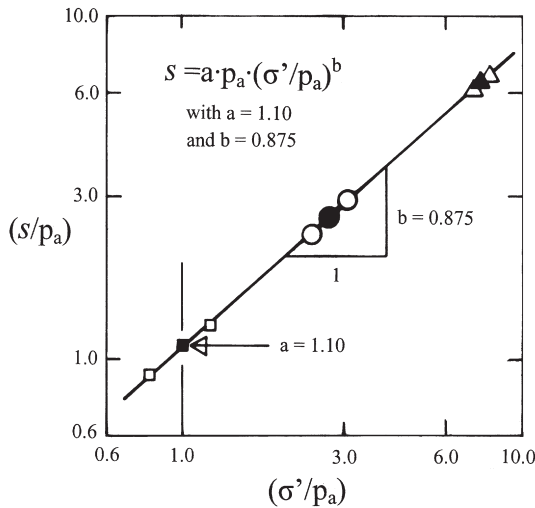
Fig. 8. Parameter determination for power function failure criterion for triaxial compression tests on dense, medium to coarse sand.

5. Surficial failure analysis with curved failure envelope

Using the power function failure criterion in Eq. (10), the factor of safety for surficial failure may be calculated from the following expression:

$$F = \frac{s}{\tau} = \frac{a \cdot p_a \cdot \left(\gamma_b \cdot h \cdot \cos^2\alpha / p_a\right)^b}{\gamma_{sat} \cdot h \cdot \cos\alpha \cdot \sin\alpha} \tag{13}$$

Using this expression, the factor of safety is compared with that obtained from Eq. (6) for a slope made of soil no. 9 for which the parameters for the two failure criteria are given in Fig. 5. The slope has an inclination of H:V = 1 1/2:1, which corresponds to $\alpha = 33.7°$. The variations of factor of safety for the two failure criteria are shown in Fig. 9. Both criteria indicate that the factor of safety vary with depth. However, the power function produces lower factors of safety for all depths, and the factor of safety reaches 1.00 at a vertical depth of approximately 2.3 m (7.5 ft). In comparison, F becomes 1.00 at a
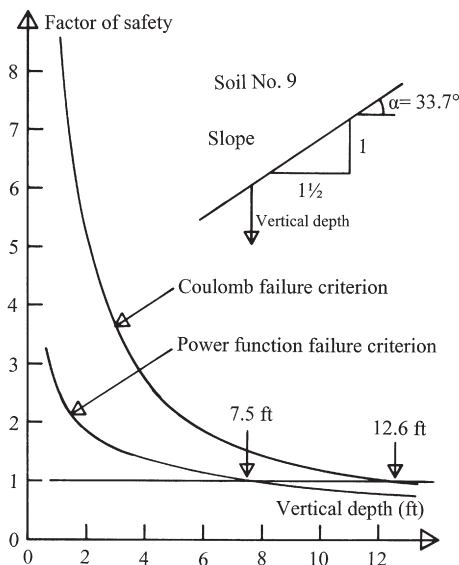
vertical depth of 3.80 m (12.6 ft) according to the Coulomb criterion. The reason for this difference is the effective cohesion which plays a major role for the stability of the slope according to the Coulomb criterion. However, as shown above, the effective cohesion is zero for non-cemented soils, and the much more realistic factor of safety for the slope is that given by the power function failure criterion.

6. Field infiltration experiments

A very instructive and carefully performed field study of water infiltration into an unsaturated expansive soil slope was reported by Ng and Zhan (2007). The test site was located in a semi-arid area in Hubei province in China, where the average rainfall is 80 cm per year with most of the precipitation distributed between May and September. Two patches, each 16 m wide and 30 m long (downslope) and sloping at 22°, were provided with sprinkler systems to simulate rainfalls and were instrumented to continuously measure water contents and suction at various locations and depths. One patch was stripped of vegetation and the other patch was overgrown by grass. The soil was a yellow–brown mottled grey clay with intermediate plasticity (LL = 49.5 and PI = 30), with cracks and fissures in the field to depths of 1.0 to 1.5 m. The test site was covered with a tarp during the rainy season preceding the experimentation, so the soil initially had a typical water content profile corresponding to the dry season, as shown schematically in Fig. 10.

Before initiation of artificial rainfall in late summer (after the rainy season), the initial matric suction in the soil was measured to be in the order of −60 kPa at a depth of 1.2 m (4 ft) and it decreased with depth to about −30 kPa at 1.8 m (6 ft). The artificial rainfall of 2.9 mm/h lasted one week. As the initially dry patches began to imbibe water, the infiltration rate initially kept up with the precipitation, i.e. all water was absorbed by the slope. However, after 1 and 1/2 day the infiltration rate began to decrease in the bare slope, while it took 3 days for reduction in infiltration rate in the grass-covered patch. Most of the remaining rainfall became surface runoff. After 7 days the infiltration rate had reduced to about 1/3 of the initial value for the bare slope, and it reduced to about 1/2 for the grass-covered slope. The difference was attributed to the larger capacity to absorb water due to the root system which provided more and deeper channels for water infiltration in the grass-covered patch.

As the water infiltrated the slope patches, it took 2.5 to 3 days for the wetting front to reach a depth of 1.6 m (5.2 ft) in the grass-

Fig. 9. Variation of factor of safety with vertical depth calculated using the Coulomb failure criterion and the power function failure criterion (1 ft = 0.305 m).
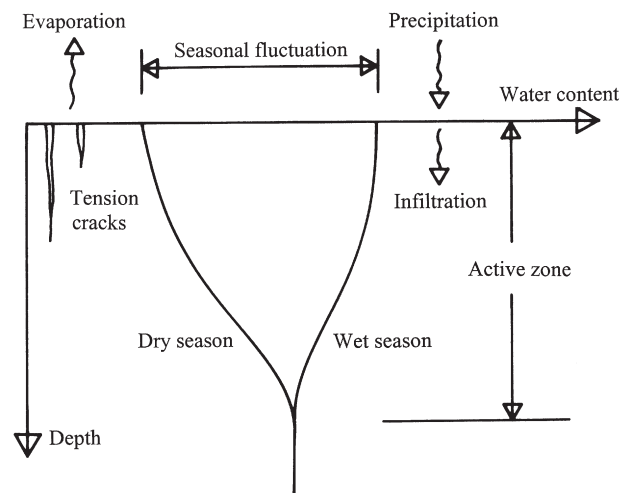
Fig. 10. Seasonal water content variation with depth in unsaturated expansive soil (after Lu and Likos, 2004).

covered area, while it took only 1.5 to 2 days to reach the same depth in the bare patch. The advance of the wetting front was followed rapidly by a conversion of the initial matric suction to a water pressure which, at a given depth, was essentially proportional to the distance to the sloping ground surface where the pressure was zero. This corresponded to the location of the ground water table where the water was free to run off. The conversion from suction to pressure took longer time in the grass-covered patch than in the bare patch where the transition was almost instantaneous as the wetting front passed a given depth in the slope.

Water content profiles after the end of the experiments looked like the one shown schematically in Fig. 10. Perched, free water was found at depths of 2.5 m for the grass-covered patch and at 1.5 m for the bare patch. Thus, the roots of surface vegetation result in higher soil suction and in greater depth of cracks and fissures, and it will cause the water to reach further down during severe rain storms, which is consistent with the higher infiltration rate in the grass-covered patch. The beneficial effect of vegetation, which is to strengthen and hold on to the soil near the ground surface, may therefore be outweighed by the ability of the water to penetrate further into the ground and reduce the factor of safety of the slope, as indicated in Fig. 9.

7. The mechanics of surficial instability

During years with little rainfall a given slope tends to dry out to a certain depth. For longer periods of several years with little rainfall the depth of the dry soil zone increases slowly. Therefore, the water content varies only in the soil close to the surface and it remains relatively constant below the zone of annual fluctuation, as shown schematically in Fig. 10. The upper dry soil layer does not reach saturation during years with regular, low precipitation.

It is the unusual large storm that produces rainfalls that saturate the upper previously dry soil layers. In the year with the large rainfall, the water keeps infiltrating into the slope as long as there is dry or almost dry soil ahead of the wetting front. As the wetting front penetrates down to the zone of relatively constant water content, the slope reaches a point of saturation and it is not capable of absorbing much more water. Thus, the impermeable layer indicated in Fig. 1 is created by the penetrating water as explained above for the field

infiltration experiments. As long as the wetting front progresses downwards, the water just behind the wetting front is under tension and provides an effective confining pressure in the soil. As the wetting front moves downwards at a slower and slower rate, the suction in the soil water changes to a positive pressure, whose magnitude quickly grows to be equal to the value given in Eq.(1).

The water in the partly saturated soil below the dry soil is under tension and this provides an effective confining pressure in the partly saturated soil. This causes the shear strength to increase in the partly saturated soil and the factor of safety will consequently increase with depths beyond the upper previously dry layer, as indicated schematically in Fig. 11. Sliding failure will occur at the level of the lowest factor of safety and this will be just above the depth to which the upper layer has previously dried out. Thus, the factor of safety does not continue to decrease as indicated by the surficial safety factor calculations, but there is a level with a minimum factor of safety at which sliding will occur.

Once the depth at which the factor of safety becomes 1.0 has been determined, it is a matter of saturating the soil to this depth before a surficial failure can happen. Since the factor of safety continues to decrease with increasing depth of water penetration, saturation of the slope to the depth where $F = 1.0$ is a matter of the initial water content in the slope and the temporal distribution of the rainfall in terms of the intensity and duration. The latter has been dealt with in detail by Pradel and Raad (1993).

8. Conclusions

For the low effective normal stresses present in surficial failure events, it is not safe to employ the Coulomb failure criterion to model the effective stress failure envelope usually determined at higher normal stresses, because there is no effective cohesion in non-cemented soils of any type. A failure criterion consisting of a simple power function is proposed here and it captures the true effective failure envelope with good accuracy and can be used in a closed form expression for the factor of safety for surficial slope failure. The suitability of this criterion is demonstrated by its fit with the experimental results obtained for various soils.

The mechanics of surficial failure is explained on the basis of a failure mode that requires saturation of the slope to the depth where the factor of safety becomes unity, observations from field rainfall infiltration experiments, and rainfalls of sufficient intensity and duration to saturate the soil to that depth. The return periods for such rainfalls in Southern California is a matter of probability as explained by Pradel and Raad (1993).

References

Abramson, L.W., Lee, T.S., Sharma, S., Boyce, G.M., 2002. Slope Stability and Stabilization MethodsSecond Edition. Wiley, New York.
Anderson, J.N., Lade, P.V., 1981. The expansion index test. Geotech. Test J. 4 (2), 58–67.
ASTM Standard Test Method D 1557 2006: Standard Test Methods for Laboratory Compaction Characteristics of Soil Using Modified Effort (56,000 ft-lbf/ft^3 (2,700 kN-m/m^3)), Annual Book of ASTM Standards, Vol. 04.08, ASTM International, West Conshohocken, PA, USA.
ASTM Standard Test Method D 4829 2006: Standard Test Method for Expansion Index of Soils, Annual Book of ASTM Standards, Vol. 04.08, ASTM International, West Conshohocken, PA, USA.
Day, R.W., Axten, G.W., 1989. Surficial stability of compacted clay slopes. Journal of Geotechnical Engineering, ASCE 115 (4), 577–580.
Duncan, J.M., Wright, S.G., 2005. Soil Strength and Slope Stability. Wiley, New York.
Hollingsworth, R., Kovacs, G.S., 1981. Soil slumps and debris flows. Prediction and protection. Bull. Assoc. Eng. Geol. 18 (1), 17–28.
Lambe, T.W., Whitman, R.V., 1969. Soil Mechanics. Wiley, New York.
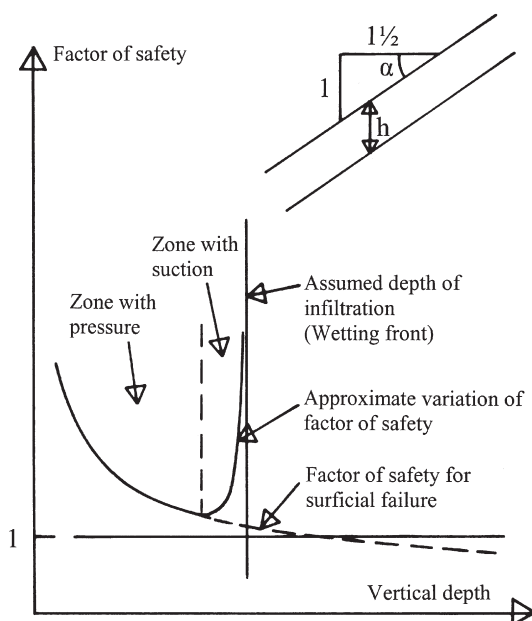
Fig. 11. Variation of the factor of safety with depth in inclined soil slope subject to water infiltration.

Lu, N., Likos, W.J., 2004. Unsaturated Soil Mechanics. Wiley, Hoboken, New Jersey.

Mitchell, J.K., Soga, K., 2005. Fundamentals of Soil BehaviorThird Edition. Wiley, New York.

Ng, C.C.W., Zhan, L.T., 2007. Comparative study of rainfall infiltration into a bare and a grassed unsaturated expansive soil slope. Soils Found. 47 (2), 207–217.

Pradel, D., Raad, G., 1993. Effect of permeability on surficial stability of homogeneous slopes. Journal of Geotechnical Engineering, ASCE 119 (2), 315–332.

Skempton, A.W., DeLory, F.A., 1957. Stability of natural slopes in Londan clay, Proc. 4th Int. Conf. Soil Mech. Found. Engrg, 2. , pp. 378–381.